Mineral. Deposita 29, 445–460 (1994)

MINERALIUM DEPOSITA

Gold mineralization in As-rich mesothermal gold ores of the Bogosu-Prestea mining district of the Ashanti Gold Belt, Ghana: remobilization of "invisible" gold

A.H. Mumin[1], M.E. Fleet[1], and S.L. Chryssoulis[2]

[1] Department of Earth Sciences, University of Western Ontario, London, Ontario N6A 5B7, Canada
[2] Amtel, University Research Park, University of Western Ontario, London, Ontario N6A 5B7, Canada

Received: 1 March 1994/Accepted: 20 June 1994

Abstract. The Bogosu-Prestea mining district of southwestern Ghana is a 33 km section of the Early Proterozoic Ashanti Gold Belt. Greenschist facies carbonaceous and carbonate-bearing turbidites and greywackes, and mafic dikes host numerous economic mesothermal gold deposits. Structurally higher ores in the Bogosu concession have brittle deformation and consist of disseminated-sulphide lodes in tectonically-disrupted sedimentary rocks and carbonate-altered mafic dikes. Most gold occurs as micrometre-size particles in arsenian pyrite, and as "invisible" gold in arsenian pyrite and arsenopyrite. The structurally deeper ores of the adjoining Prestea concession are associated with brittle-ductile deformation and consist of extensive crack-seal quartz-veins and graphitic shear zones. Only minor amounts of "invisible" gold were detected; in these deeper lodes, gold occurs dominantly as abundant microscopic and larger particles in sulphide/arsenide minerals and in gangue. The gold distribution patterns revealed by SIMS microprobe analysis and ion maps, EMP and colour staining suggest that most of the primary gold in the Bogosu-Prestea system precipitated in solid-solution with sulphide/arsenide minerals. However, post-depositional concentration and redistribution occurred, in increasing degree with: 1) increase in metamorphic/hydrothermal gradients in the gold system (depth), 2) decrease in the refractory properties of the host mineral, and 3) increase in the amount of post-depositional, host-mineral recrystallization and deformation. Gold evolved from primary solid-solution within sulphide/arsenide minerals, to colloidal and micrometre-size particles concentrated in voids, fractures and internal grain boundaries, and finally to microscopic and larger particles at sulphide/arsenide grain margins and in the gangue assemblage. The general conclusions presented here are applicable to As-rich gold deposits of all ages, worldwide. The presence of gold in late fractures is insufficient evidence for late-stage introduction of gold in mesothermal gold systems.

In recent years the presence of "invisible" gold in ore minerals has been documented from numerous gold mines worldwide, including Elmtree (N.B., Canada), Agnico Eagle (Canada), Fairview (South Africa), Sheba (South Africa), Red Lake (Canada), Carlin (USA), and Chatelet and Villeranges (Massif Central, France) (Cathelineau et al. 1989; Cabri et al. 1989; Bakken et al. 1989; Cook and Chryssoulis 1990; Chryssoulis and Cabri 1990; Fleet et al. 1993). These previous studies have demonstrated a direct correlation of gold-deposition with As-rich growth bands in both pyrite and arsenopyrite, and suggested several possible methods by which this might occur. Other investigators, such as Bonnemaison and Marcoux (1990), have proposed a multi-state formation of auriferous deposits. Based on studies from France, West Africa and South America, they propose that gold mineralization began with the precipitation of "invisible" gold in pyrrhotite and its subsequent dissolution and fixation in the matrix of later pyrite, arsenopyrite and quartz.

This paper documents gold mineralization in the large Bogosu-Prestea mesothermal lode gold system of the Ashanti Gold Belt, Ghana. In particular, we report features that may be important links in the history of the deposition and evolution of mesothermal gold deposits, including: 1) the intimate relationships between solid-solution, colloidal, microscopic and visible gold, and the sulphide and arsenide minerals with which these forms of gold are associated, and 2) the effects that depth of mineralization, mineral phase and hydrothermal/metamorphic history have on the post-depositional evolution of gold. Finally, new constraints on the timing and mechanism of gold precipitation and the evolution of gold morphology, grain size and siting are discussed.

Geology, history of alteration and gold mineralization

The Bogosu-Prestea mesothermal lode deposits are part of a large gold system in the Ashanti Structural Belt that is well-constrained in respect to geological, geochemical, hydrothermal and metamorphic parameters. The Ashanti Gold Belt is by far the most important gold-bearing structure of the Early Proterozoic (2.3–2.0 Ga) Birimian rocks of West Africa (Fig. 1). The Birimian covers a large area of southern West Africa, including parts of Cote D'Ivoire, Ghana, Burkina Faso, Guinea, Liberia, Mali and Senegal. In

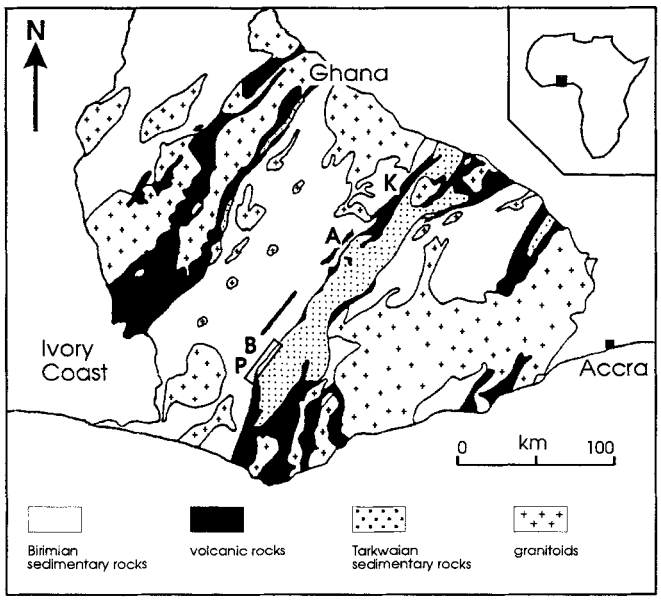

Fig. 1. Location map and Birimian geology of southwestern Ghana. *PBAK* is the location of the Ashanti Gold Belt; *P* is the Prestea mining district; *B* is the Bogosu mining district; *A* is the Obuasi mining district and *K* is the Konongo mining district

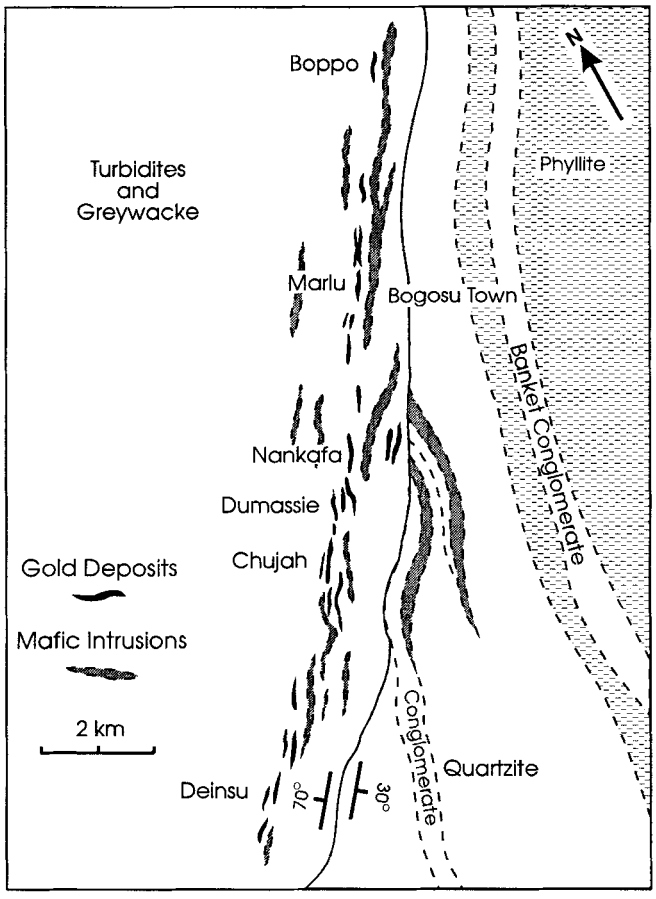

Fig. 2. Geology and location map for gold deposits of the Bogosu mining district

southwestern Ghana, the Birimian is comprised of 4 major units: marine sedimentary rocks, volcanic greenstone belts, granitoid intrusions and younger clastic sedimentary rocks (Tarkwaian). All units are aligned in N-S to NE-SW structural belts (Junner 1940; Hastings 1982; Kesse 1985; Luebe et al. 1990; Taylor et al. 1992; Milesi et al. 1992; Mumin 1994; Fig. 1). We presently consider that the host rocks of the Ashanti Gold Belt formed by subduction driven accretion of sedimentary rocks onto the West African craton (Mumin, 1994). Primary lode gold ores were deposited in major and minor structural lineaments parallel to volcanic belts, and quartz-pebble conglomerate paleoplacers and modern placers resulted from erosion and reconcentration of primary deposits (Sestini 1973; Abouchami et al. 1990; Luebe et al. 1990; Milesi et al. 1992; Taylor et al. 1992; Klemd et al. 1993; Mumin 1994).

The Bogosu and Prestea mining concessions are located in southwestern Ghana 60 to 90 km northeast of the Atlantic coast line at Axim (Fig. 1). The Ashanti Gold Belt strikes through the centre of these concessions for 33 km; 18 km in the Bogosu concession (Fig. 2) and 15 km in the Prestea concession, immediately to the southwest. This region, with more than 230 tonnes of gold produced, is the southern-most of three major mining districts along the Ashanti Gold Belt. The Obuasi area in the central portion, which is mined by Ashanti Goldfields Limited, has produced to date over 700 tonnes of gold, and the Konogo district, about 250 km northeast of the coast near the northeastern-most extremity of the belt, has produced about 60 tonnes of gold.

The geology of the Bogosu and Prestea mining concessions has been described by Adjimah (1988), Appiah et al. (1991) and Mumin (1994). In the Bogosu and Prestea mining district, the Ashanti structural zone disrupts Birimian phyllitic turbidites and greywackes immediately east of the contact with later clastic sediments of the Tarkwaian sequence. The structural zone is approximately 1 km wide and is intruded by numerous dikes of variable but mostly mafic composition. It is ubiquitously enriched in gold and hosts numerous large-to-small mesothermal gold deposits throughout the two concessions. The deposits grade from brittle-shear-zone hosted disseminated sulphide lodes at Bogosu, to structurally deeper brittle-ductile ores in the central Prestea area (Mumin 1994; Fig. 3). The structurally deeper ores are dominated by large, crack-seal quartz veins with disseminated sulphides along ribbons of wall-rock included in the quartz, and by sheared hanging-wall, footwall and country rocks. In the structurally higher ores, both the host sedimentary-rocks and to a lesser extent the mafic dikes form gold ores. In Bogosu ores the mineralization is dominated by Au-bearing arsenian pyrite and arsenopyrite, and in the structurally deeper Prestea ores by Au-bearing arsenopyrite, arsenian pyrite, chalcopyrite, sphalerite, gangue and to a minor extent tetrahedrite and other trace sulphides.

Near-surface oxidized ores on the Bogosu concession were mined by a series of shallow open pits between 1934 and 1954 by Marlu Gold Mining Areas Limited. The gold was recovered by cyanide leaching. Mining in the Bogosu concession was resumed in 1990 by an international consortium led by Billiton International Metals BV. Open pit methods are being used to extract the sulphide ores below the zone of oxidation. These refractory ores are roasted prior to cyanide leaching. Total production to date from the Bogosu concession exceeds 40 tonnes of gold. The underground workings of the Prestea concession extend for about 8 km along strike and to a depth of about 1.7 km. The Prestea mines are currently operated by Prestea Goldfields Limited and have been in production for about 100 years. Gravity techniques are used to recover about 60% of the gold which is free-milling, while the remaining 40% of production is by roasting and cyanide-leaching of refractory particulate gold from sulphide and arsenide minerals. Total production from the Prestea mines exceed 190 tonnes of gold. In addition, about 30 tonnes of gold (recorded production) has been dredged from the Ankobra river which drains the Ashanti Gold Belt in the Bogosu-Prestea district, and abundant unrecorded gold winning by local entrepreneurs, dating from historical times, continues to the present day (Kesse 1985; Knopf 1988; Garard 1989).

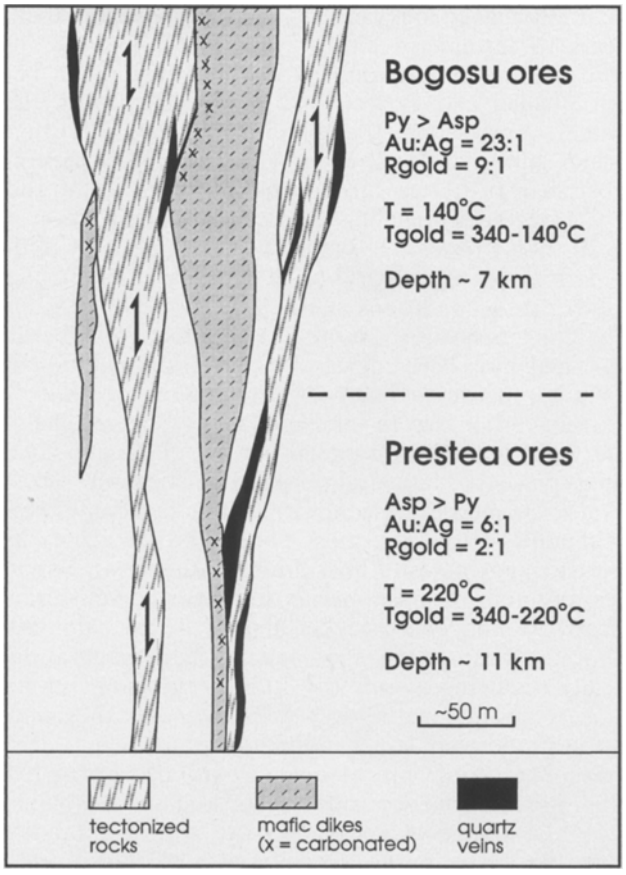

Fig. 3. Schematic cross-section and interpretation of the geology of the Ashanti Gold Belt in the Bogosu-Prestea mining district. Cataclastic ores are exposed on the Bogosu concession and structurally deeper brittle-ductile ores are found in the Prestea concession. Host rocks are Birimian turbidites and greywackes. Depth estimates are based on ambient hostrock temperatures at the time of gold deposition from carbonate mineral geothermometry and a geothermal gradient of 20 °C per km depth (Mumin and Fleet 1994). Individual tectonized and mineralized zones range up to 50 m in width, and form a series of sub-parallel lenses within the 1 km wide Ashanti Structural Belt. R_{gold} is the ratio of gold associated with sulphide/arsenide minerals to gold in gangue; T is the ambient country-rock temperature during gold deposition; T_{gold} is temperature of hydrothermal fluids during gold deposition

The ore deposits of the Ashanti Gold Belt are similar to turbidite-hosted mesothermal lode gold deposits in other parts of the world (cf. Sandiford and Keays 1986, Ballarat Slate Belt, Victoria; Haynes 1986, Kontak and Smith 1993, Meguma Terrane, Nova Scotia; Goldfarb et al. 1989, 1991, Alaska-Juneau deposits). Country-rocks of the Bogosu-Prestea mining district have been metamorphosed to a chlorite-epidote-carbonate-quartz-sericite-rutile greenschist facies assemblage. Ankerite and siderite occur in sedimentary rocks, and calcite occurs in the least-altered mafic dikes. Significant bleached zones of ankerite-siderite-sericite-quartz wall-rock alteration occur in the mafic lithologies. However, in spite of the presence of abundant carbonate minerals and sericite, distinct zones of hydrothermal wall-rock alteration do not occur in the host turbidites and greywackes. The gangue mineralogy of the ore deposits is dominated by quartz, ankerite, sericite, albite, siderite, and rutile.

The Ashanti Gold Belt developed as a compressional structure of regional extent during the tectonic/metamorphic history of the Birimian rocks of southwestern Ghana (Taylor et al. 1992; Mumin 1994; Mumin and Fleet, 1994). However, only during periods of relaxation of the tectonic forces did the Ashanti Structural Belt become a dilatant feature and the principal conduit for fluids generated in the region. Gold mineralization is interpreted to have formed at these times, during active uplift late in the history of the Belt (cf. Kerrich and Wyman 1990).

The compositions of siderite, ankerite and calcite and stable isotope characteristics suggest that generation of ore fluid occurred at depth below the gold deposits as a result of metamorphic decarbonation and dehydration reactions (Mumin 1994; Mumin et al. 1994). Gold deposition occurred over a temperature range of approximately 340 to 140 °C, at higher levels in the structural conduit, where ambient temperatures of country rocks were 140 and 220 °C for Bogosu and Prestea ores, respectively. Consequently, the ore deposits have a post-peak-metamorphic signature that is characteristic of many mesothermal gold deposits worldwide. Fluid activity was episodic, with pulses of hot fluid periodically surging upward, reacting with and overprinting earlier-formed mineral assemblages within and proximal to the conduit (Mumin 1994; Mumin et al. 1994).

Experimental

Sampling and mapping of the Bogosu-Prestea mining district commenced in 1988. Sampling from the Prestea concession was restricted to available underground exposures, particularly on the 17 and 22 levels ($\approx$ 750 m and 1000 m vertical depth, respectively) of the Prestea Goldfields Limited mine. At Bogosu, samples of diamond drill core were taken from the Bogosu South area (Marlu south area), Nankafa deposit, Dumasie and Dumasie East deposits, and various deposits of the Chujah area (Fig. 2). Samples were collected from all the important varieties of host, altered and mineralized rock types. However, due to the extent of the structural zone ($\approx$ 1 km width) and the lack of rock exposure outside the mine workings, no samples were collected beyond the limits of the Ashanti Structural Belt.

Approximately 90 polished thin sections were examined by transmitted and reflected light microscopy. Of these, 42 sections were systematically scanned for size and distribution of microscopic gold particles. Reconnaissance work on arsenian pyrite and arsenopyrite in several of these sections used the permanganate staining technique of Fleet et al. (1989, 1993).

Individual grains of arsenian pyrite, arsenopyrite, tetrahedrite and gold from 8 polished thin sections were analyzed by EMP for Fe, As, Ni, Cu, Zn, Pb, Co, Sb, Au, Ag and Hg using a JEOL JXA-8600 Superprobe, operated at 20 kV, 50 nA, with natural pyrite (Fe, S), arsenopyrite (As), tetrahedrite (Fe, As, S, Sb, Cu) and cinnabar (Hg), synthetic NiS (Ni), pure chalcopyrite (Cu) and sphalerite (Zn) and pure Co, Ag and Au as standards. Gold was analysed using the AuMα line, 100-s counts, and with one spectrometer dedicated entirely to Au.

The distribution of gold in arsenian pyrite and arsenopyrite was confirmed and quantified by SIMS. This method has been routinely used to quantify the "invisible" Au content and colloidal-size Au in pyrite and arsenopyrite (Cook and Chrysoulis 1990; Fleet et al. 1993). Thirty analyses of 10 pyrite and 13 arsenopyrite grains from two ore samples taken from the Prestea and Bogosu mines were obtained (Table 6). Samples were analyzed using an upgraded Cameca IMS-3f ion microprobe for ^{197}Au, ^{75}As, ^{56}Fe and ^{34}S. Operating conditions are detailed in Fleet et al. (1993).

Ion mapping by SIMS was used to further characterize the distribution of sub-microscopic gold within individual arsenian pyrite and arsenopyrite grains. Thirty-nine images of ^{34}S, ^{75}As, and ^{197}Au distribution were obtained from 8 grains. Ion mapping was performed by electronically rastering the primary beam over an area of 250 × 250 μm; further details are given in Fleet et al. (1993).

Ore mineralogy and paragenesis

Ore minerals in the Bogosu-Prestea mining district include arsenian pyrite, arsenopyrite, pyrite, pyrrhotite,

marcasite, chalcopyrite, sphalerite and trace amounts of tetrahedrite, galena, stibnite, cobaltite, gersdorffite, boulangerite and ullmanite. Gold in the Bogosu-Prestea system is present as: 1) visible gold (> 100 μm) in quartz, albite and carbonate; 2) microscopic gold (> 0.1 to < 100 μm) associated with sulphide minerals and interstitial to silicates; and 3) "invisible" gold (< 0.1 μm). The latter association is comprised of: 1) gold in solid solution within the crystal lattice of sulphide and sulphide/arsenide minerals; and 2) colloidal-size inclusions within sulphide and sulphide/arsenide minerals.

Sulphide/arsenide minerals are intimately associated with gold deposition throughout the Bogosu and Prestea districts. We presently recognize four stages of hydrothermal alteration and ore mineral deposition (Fig. 4) based on the paragenetic sequence of sulphide/arsenide minerals in the gold lodes.

Stage 1 minerals pre-date gold deposition, occurring ubiquitously as minor amounts (< 1%) of finely disseminated anhedral to euhedral pyrite with trace amounts of chalcopyrite in least-altered sedimentary and mafic rocks of the Ashanti Gold Belt. Their origin may be as early as diagenesis or as late as prograde metamorphism and deformation.

Stage 2 mineral assemblages are related to the onset of gold mineralization and are dominated by pyrrhotite, marcasite and pyrite. Up to several modal percent anhedral grains of pyrrhotite occur most commonly along carbonaceous shear planes in host-rocks and ores of the Prestea concession, but ore textures suggest that pyrrhotite was formerly more abundant and has been partly altered to randomly oriented marcasite and pyrite, particularly along fractures and grain margins. In the structurally higher rocks of the Bogosu concession, there appears to have been almost complete conversion of pyrrhotite to marcasite and pyrite. This distinction between Bogosu and Prestea ores is consistent with the carbonate geothermometry (Mumin and Fleet, 1994), that indicates lower ambient country-rock temperatures at Bogosu than at Prestea during mineralization (≈ 140 and 220 °C, respectively), shallower depths of mineralization at Bogosu than Prestea (≈ 7 and 11 km, respectively; estimated assuming a geotherm of 20 °C per km depth), and more oxidizing conditions at Bogosu.

The conversion of pyrrhotite to marcasite and pyrite (Fig. 4) may have been coeval with partial sulphidation of siderite ± ankerite to finely disseminated pyrite microcrystals in carbonates. In some moderately sheared shaly- or slaty-phyllites, several modal percent of disseminated pyrite is present as anhedral porphyroblastic grains up to several millimeters in size and with quartz-carbonate pressure shadows. However, most Stage 2 pyrite occurs as cataclastic aggregates of finer grains along shear planes. Trace amounts of arsenopyrite. tetrahedrite, sphalerite, chalcopyrite and cobalt-nickel arsenides and sulphides also formed during late Stage 2 or early Stage 3 alteration, typically occurring as tiny (< 0.1 mm) inclusions in arsenian pyrite, but in the deeper Prestea ores they may occur as moderately larger individual grains.

Stage 3 minerals are associated with the main hydrothermal and gold deposition event, and are dominated by the assemblage of arsenian pyrite and arsenopyrite (Fig. 5). Arsenian pyrite commonly nucleates around earlier As-poor pyrite (Figs. 5C, 5E and 5F), and forms porphyroblastic grains up to 2 mm in size, with inclusions of acicular arsenopyrite.

The abundance of sulphide and arsenide minerals varies with ore type and location. Sedimentary-rock hosted ores contain from 2 to 15 modal% sulphides with arsenian pyrite dominating, while mafic-rock hosted ores typically

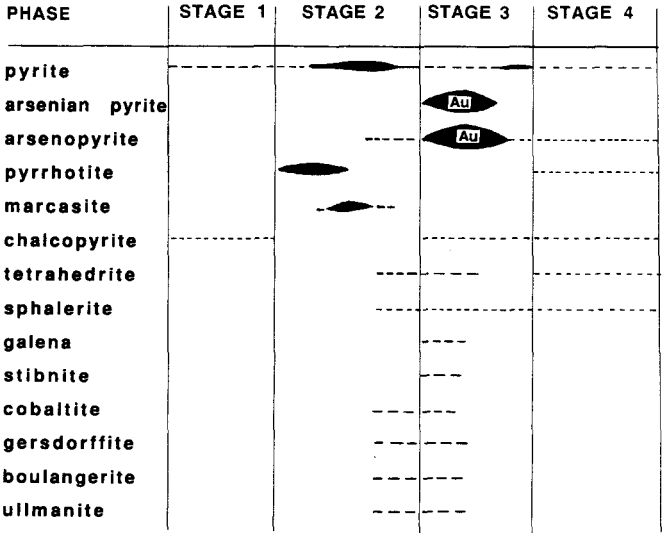

Fig. 4. Paragenetic sequence for sulphide and arsenide minerals in Bogosu and Prestea ores and host-rocks. *Stage 1* Early sulphide minerals that pre-date hydrothermal alteration related to gold deposition. *Stage 2* Sulphide minerals that precipitated from the gold-bearing hydrothermal fluids prior to gold deposition. *Stage 3* Sulphide/arsenide minerals that are contemporaneous with gold deposition. *Stage 4* Sulphide/arsenide minerals that formed after precipitation of gold

Fig. 5A–F. EMP back-scattered electron images of gold-bearing arsenian pyrite and arsenopyrite from Bogosu and Prestea ores. *Asp-(s.t.)* sieve-textured arsenopyrite; *Py-(s.t.)* sieve-textured pyrite; *Py-(As)* arsenian pyrite. **A** Abundant gold particles within the sieve-texture core of an arsenopyrite grain. Note, also the accumulation of gold along fractures. The sieve-textured core is thought to result from the alteration of early pyrrhotite to marcasite, pyrite and finally arsenopyrite. Sample P-9 is from the Main Reef quartz vein in the Prestea mine. **B** Rhythmic compositional zoning of arsenian pyrite. *Lighter bands* are As-rich. Sample P-2 is from the Main Reef quartz vein in the Prestea mine. **C** Complex compositional zoning and recrystallization in a porphyroblastic arsenian pyrite grain. Early As-poor pyrite crystals were cemented together and overgrown by arsenian pyrite. The larger arsenopyrite crystals were included during growth of the pyrite grain. Microcrystals of pyrite, pyrrhotite and arsenopyrite formed during late recrystallization of the arsenian pyrite. Gold content (ppm) by SIMS is shown for 3 areas. Sample DM-11 is from a carbonated-dike ore from the Dumassie deposit, Bogosu concession. **D** Detail of the recrystallized portion of the arsenian pyrite crystal shown in Fig. 5C. **E** Detail of the sieve-textured (*s.t.*) core of the arsenian pyrite crystal shown in Fig. 5C. **F** Compositional zoning in an arsenian pyrite grain from carbonated-dike ore from the Chujah deposit (sample C-11). The sieve-textured core is believed to be an alteration of pyrrhotite and marcasite. Numbers 11 to 13 are the locations of EMP analyses listed in Table 2

contain from 3 to 20 modal% sulphides with a greater proportion of arsenopyrite. In Bogosu ores arsenian pyrite is the dominant sulphide, whereas disseminated fine-grained needles of arsenopyrite (typically < 0.2 mm in length) make up the balance of sulphide/arsenide minerals. In the structurally deeper ores from Prestea arsenopyrite is more abundant than arsenian pyrite, and has a fine to medium grain size (up to 5 mm in length). Crack-seal quartz veins of the structurally deeper ores contain mostly arsenopyrite with minor amounts of arsenian

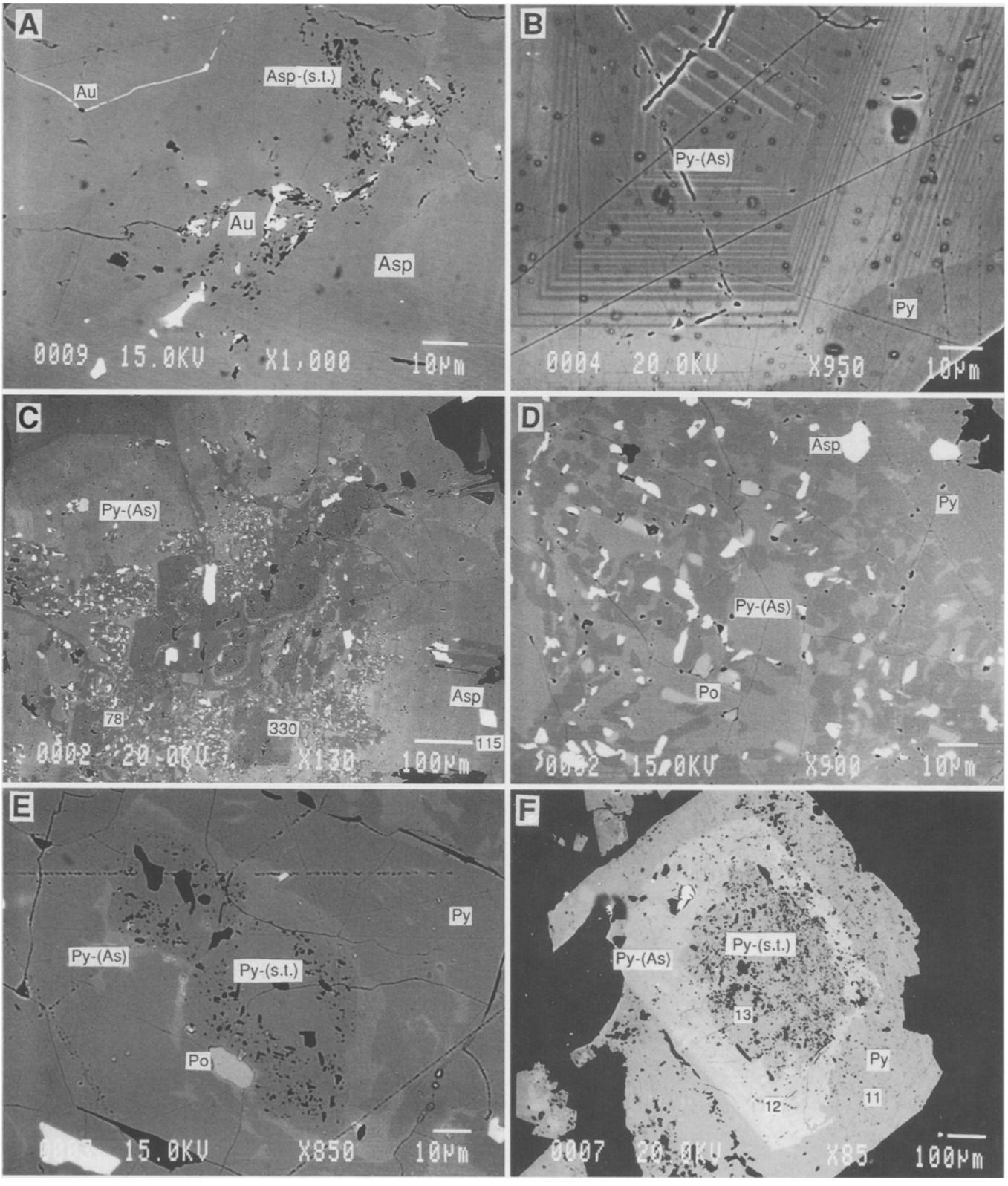

pyrite, sphalerite, chalcopyrite, tetrahedrite and other minor sulphides disseminated along ribbons of wall-rock within the quartz lode.

Rhythmic compositional zoning caused by variation in As content is typical of arsenian pyrite from the structurally deeper ores at Prestea (Fig. 5B). However, in the structurally higher Bogosu ores, a complex microstructure is commonly observed in pyrite porphyroblasts consisting of from core to rim: 1) sieve-textured, As-poor core believed to have altered from early pyrrhotite and marcasite, 2) a broad zone of arsenian pyrite, and 3) grain margin of normal, As-poor pyrite (Figs. 5C and 5F). The characteristic rhythmic zonation of Prestea pyrite contrasts with the single apparently uniform broad zone of As-rich pyrite from Bogosu; however, at higher resolution, the broad As-rich bands in Bogosu pyrite are seen to be composed of a very fine-scale compositional zoning. This difference in arsenian pyrite is believed to reflect subtle differences in hydrodynamic conditions and local equilibrium. Distinct pulses of hydrothermal fluid may enter the system in the structurally deeper levels, and become compositionally more diffuse as they migrate to structurally higher levels in the gold system. Alternatively, episodic phase separation may cause variations in the hydrodynamic equilibrium sufficient to induce rhythmic precipitation of As-rich minerals.

Acicular and often compositionally-banded arsenopyrite crystals are common in both Bogosu and Prestea ores. Some arsenopyrite grains from Prestea (Figs. 6D and 6E) appear to have nucleated on early grains of iron sulphide (pyrrhotite, marcasite, pyrite).

Stage 4 deposition of sulphide/arsenide minerals occurred after the main gold event. Only trace amounts of ore minerals formed at this time including: pyrite, arsenopyrite, pyrrhotite, chalcopyrite, tetrahedrite, sphalerite and possibly some of the other trace sulphide/arsenide minerals that occur sporadically. Pyrite forms a late margin to arsenian pyrite grains, but most of the other late minerals are believed to have formed from recrystallization of metastable arsenian pyrite (e.g., Figs. 5C and 5D). The complex pyrite grain shown in Figure 5C is composed of an As-poor core surrounded by a metastable, As-rich zone (up to > 5 wt % As) that gradually decreases in As content toward the margin of the grain. Zones with high As content recrystallized to form arsenopyrite and pyrrhotite microcrystals in a mosaic of As-poor pyrite.

The crystallization of arsenopyrite and pyrrhotite from arsenian pyrite suggests a similar origin for some of the other sulphide phases that occur as micrometer-sized inclusions within arsenian pyrite (e.g. tetrahedrite, chalcopyrite, sphalerite, stibnite, cobaltite, gersdorffite, boulangerite). This is supported by elevated levels of zinc, copper, antimony, cobalt, nickel, and lead within certain growth zones of arsenian pyrite and arsenopyrite grains (Tables 1 and 2). Alternatively, these minor ore mineral phases could pre-date formation of pyrite poikiloblasts.

Arsenopyrite geothermometry (Kretschmar and Scott 1976; Sharp et al. 1985) yields temperatures for the main hydrothermal event (Stage 3) of < 300 to ≈ 450 °C for coexisting arsenopyrite and arsenian pyrite and < 300 to 410 °C for gold-bearing arsenopyrites. These temperatures for ore mineralization compare favourably with temperatures deduced from the mineral chemistry of carbonates (Mumin and Fleet 1994).

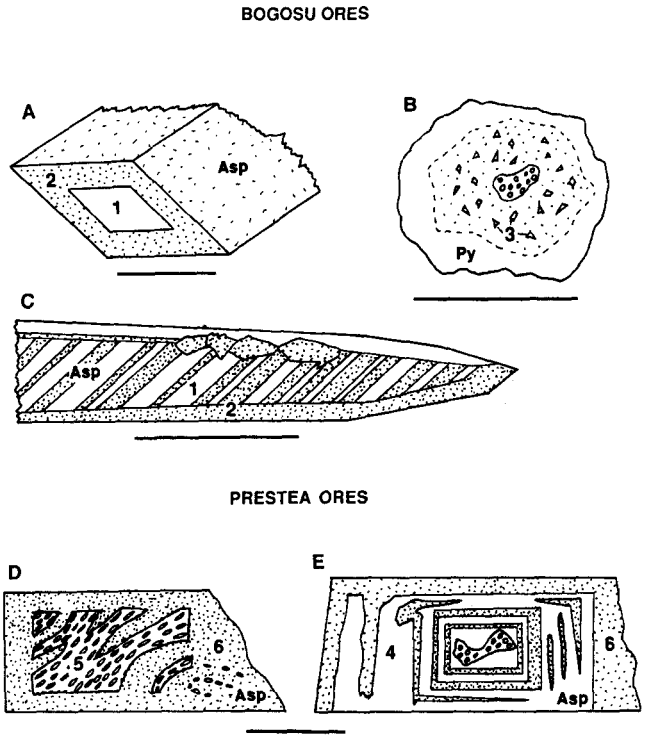

Fig. 6A–E. Sketches of compositional and textural zoning of arsenopyrite grains from Bogosu and Prestea ores: composition in at% As: *1* 30.7 ± 0.2, Au-rich, $n = 2$; *2* 32.7 ± 0.7, Au-poor, $n = 6$; *3* 32.5 ± 0.4, Au-poor, $n = 4$, recrystallized from arsenian pyrite; *4* 29.1 ± 0.1, Au-rich, $n = 3$; *5* 30.2, Au-poor, $n = 1$, altered from pyrite and marcasite; *6* 31.6 ± 0.3, Au-rich, $n = 7$ and 34.0 ± 0.4, Au-poor, $n = 2$. Scale bar: **A**, **C**, **D** and **E** 0.1 mm, **B** 1.0 mm

Microscopic gold

In all ore types at Bogosu, gold occurs predominantly as microscopic inclusions within pyrite. Individual grains range from < 1 μm to a maximum observed size of 35 μm. Occasionally, small grains occur within arsenopyrite crystals or in gangue minerals. Consequently, the Bogosu ores are highly refractory unless oxidized by surface weathering.

Although veinlets of native gold do occur within Prestea quartz-vein lodes, the vast majority of free-milling gold occurs as < 100 μm size grains along fine ribbons of wall-rock within quartz, and in adjacent graphitic fissure ores (shears). These wall-rock partings also are the locus of abundant fine-grained sulphides that are frequently intimately associated with the gold. Gold most commonly is associated with arsenopyrite and/or arsenian pyrite, or it occurs as free grains in the quartz-albite-ankerite gangue along the wall-rock partings. Occasionally gold is enclosed within or at and near the margins of chalcopyrite and sphalerite grains. In mineralized sedimentary rocks and graphitic fissure zones, gold occurs as 1 to 50 μm size

Table 1. Mineral chemistry of selected arsenopyrite grains (EMP wt %)

Sample	Fe	As	S	Ni	Cu	Co	Sb	Au	Total	Comment
C-11-1	34.5	44.5	19.3	0.04	ND	0.32	0.03	0.00	98.7	
C-11-1	35.1	42.9	21.6	0.38	ND	0.15	0.00	0.02	100.1	
C-11-9	33.9	44.9	19.8	0.17	ND	0.80	0.05	0.00	99.5	
D-10-5	35.0	44.4	20.2	0.15	ND	0.03	0.00	0.00	99.8	
DM-3-4	33.2	45.3	20.9	0.02	0.03	0.01	0.01	0.02	99.4	
DM-11-6b	32.7	44.8	21.1	1.05	0.06	0.03	0.04	0.00	99.8	μ-xtal
DM-11-6c	31.9	45.1	20.9	0.23	0.00	0.01	0.10	0.00	98.2	μ-xtal
DM-11-7b	32.0	45.4	20.5	0.08	0.02	0.00	0.15	0.06	98.3	Incl.
DM-11-7c	32.2	44.9	21.0	0.18	0.01	0.60	0.06	0.00	98.8	μ-xtal
DM-11-8	31.9	42.6	22.5	0.00	0.00	0.00	0.00	0.07	97.0	Core
DM-11-8	32.9	46.1	20.3	0.07	0.01	0.11	0.02	0.00	99.5	Margin
P-2-1	35.4	43.9	20.4	0.06	ND	0.00	0.00	0.00	99.7	
P-2-1	35.8	44.3	20.6	0.02	ND	0.00	0.01	0.04	100.7	
P-2-1	36.2	41.4	22.5	0.02	ND	0.03	0.00	0.02	100.2	
P-2-1	35.1	43.3	20.5	0.10	ND	0.16	ND	0.00	99.1	
P-19-7	34.7	44.7	20.3	0.12	ND	0.13	0.01	0.02	100.0	Margin
P-19-7	35.8	41.7	22.5	0.02	ND	0.03	0.02	0.00	100.0	Middle
P-19-7	35.5	44.5	20.5	0.00	ND	0.00	0.01	0.00	100.5	Core
P-28 D-5	33.2	43.8	22.2	0.01	0.02	0.04	0.00	0.05	99.3	
P-28 D-5	32.0	47.2	19.6	0.04	0.01	1.08	0.08	0.05	100.1	Margin
P-28 D-5	35.7	42.1	23.2	0.01	0.00	0.00	0.03	0.00	100.9	
P-30-6a	32.4	43.3	20.8	0.97	0.00	0.02	0.00	0.00	97.5	
P-30-6b	35.8	43.3	22.3	0.01	0.00	0.00	0.00	0.03	101.4	Alt. core
P-30-6b	35.1	47.4	19.9	0.12	0.00	0.11	0.00	0.07	102.8	Margin

C, Chujah deposit, Bogosu; D, DM, Dumassie deposit, Bogosu; P, Prestea mine
Incl., inclusion in pyrite; Alt., altered from pyrrhotite, marcasite and pyrite
ND, no data; μ-xtal, recrystallized microcrystal in pyrite

Table 2. Mineral chemistry of selected pyrite grains (EMP wt %)

Sample	Fe	As	S	Ni	Co	Au	Total
C-11-11	45.5	0.0	53.0	0.00	0.02	0.00	98.6
C-11-12	45.6	3.6	50.1	0.00	0.00	0.00	99.3
C-11-13	46.6	0.0	53.4	0.02	0.00	0.00	100.1
P-19-37	45.6	0.1	52.9	0.00	0.20	0.00	98.9
P-19-38	46.1	0.5	53.2	0.03	0.06	0.00	99.9
P-19-39	45.5	1.5	52.6	0.50	0.09	0.00	100.2
P-19-40	46.0	0.7	52.7	0.01	0.08	0.04	99.6
P-19-41	45.4	1.6	52.6	0.60	0.21	0.00	100.4
P-19-42	45.9	1.2	52.5	0.03	0.00	0.00	99.6
P-19-43	45.9	0.9	53.2	0.01	0.00	0.02	100.0
P-19-44	46.2	0.3	52.1	0.08	0.00	0.00	98.6
P-19-45	46.1	0.1	53.1	0.01	0.00	0.00	99.3
P-19-46	46.5	1.0	52.6	0.00	0.00	0.00	100.0
P-19-47	46.3	0.9	52.6	0.00	0.00	0.00	99.7
P-19-48	45.3	1.6	52.4	0.71	0.05	0.03	100.1
P-19-49	46.2	0.4	52.9	0.00	0.03	0.03	99.5
P-19-50	46.0	0.9	52.6	0.01	0.00	0.00	99.5
P-19-51	46.2	0.3	52.9	0.01	0.05	0.00	99.5
P-19-52	46.1	0.6	53.0	0.07	0.00	0.00	99.8
P-19-53	43.0	0.3	49.1	0.08	0.09	0.00	92.6
P-19-54	46.4	0.1	53.5	0.04	0.07	0.00	100.0
P-19-55	46.5	0.1	53.3	0.02	0.13	0.00	100.0
P-19-56	46.0	0.0	53.9	0.04	0.00	0.03	100.1
P-19-57	45.9	1.4	52.0	0.56	0.10	0.00	99.9

C, Chujah deposit, Bogosu; P, Prestea mine

inclusions within pyrite and/or arsenopyrite, and to a lesser extent within gangue minerals. Generally, microscopic inclusions of gold occur within voids and fractures in sulphides, or along common grain boundaries of sulphides (Fig. 5A). In mineralized dikes at Prestea, gold is restricted almost exclusively as inclusions within arsenopyrite and pyrite.

Of the forty-two polished thin sections of Bogosu and Prestea ores examined, thirty contained detectable microscopic gold grains ranging from 0.5 to 92 μm in longest

dimension. Individual sections contained from none to 110 grains of gold for a total of 563 grains that were counted and categorized according to size and distribution (Table 3).

At Bogosu, 90% of the microscopic gold is directly associated with pyrite and arsenopyrite, with the remaining 10% interstitial to quartz, albite and carbonate gangue (Table 3). Approximately 89% of the sulphide-associated gold occurs with arsenian pyrite, and most of it is enclosed within voids and fractures (95%). The recorded size range of gold particles at Bogosu was 0.5 to 35 μm, with an average grain size of about 7 μm (longest dimension). Gold is coarser grained in the structurally deeper Prestea ores. The recorded size range of microscopic gold particles less than 100 μm, was from 0.5 to 92 μm, with an average grain size of 8 μm. In polished section, only 67% of Prestea gold grains are directly in contact with sulphide grains while the remaining 33% are interstitial to quartz, albite and carbonate gangue minerals. Fifty percent of the recorded sulphide-associated gold occurs with arsenopyrite, 31% with pyrite and 19% with other sulphides such as chalcopyrite, sphalerite and rarely, tetrahedrite and pyrrhotite. Seventy eight percent of these gold grains are in voids and fractures within sulphide grains while the remaining 22% are at grain margins. Much of the observed arsenopyrite-hosted gold from Prestea occurs as anhedral inclusions in the spongy sieve-textured core of grains (Fig. 5A). As noted above, these spongy core areas result from conversion and subsequent alteration of earlier sulphides (cf., Murowchick 1992) and apparently were efficient traps for the accumulation of gold particles.

Mineral chemistry of gold and tetrahedrite

Electron microprobe analyses of 27 grains of gold from the main ore types at Bogosu and Prestea reveal the gold to be silver-bearing. However, the Au/Ag ratio varies significantly between ore types and mining districts. Measured Ag concentrations in gold ranged from 1.2 to 7.6 wt % at Bogosu, and 7.6 to 21.3 wt % at Prestea, with average Au/Ag ratios of 23:1 and 5:1, respectively (Tables 3 and 4). The highest Ag values were observed in gold from the sedimentary-rock hosted ores and quartz-vein ores, while gold from the mineralized dikes has the lowest Ag content. The average Ag concentration is 3.3 and 6.6 wt % for analysed gold grains in Bogosu dike-ores and sedimentary-rock ores (graphitic crush zones), respectively. At Prestea, mineralized dikes average 11.5 wt % Ag, while higher concentrations averaging 18.5 wt % Ag occur in gold grains from quartz lodes and sedimentary-rock hosted ores (Fig. 7). Copper concentrations in gold grains are similar for both areas, averaging about 0.1 wt %. However, the average Hg concentration in gold grains from the Bogosu ores is moderately higher (0.5 wt % Hg) compared to the Prestea ores (0.3 wt % Hg).

Trace amounts of tetrahedrite containing Ag and Au were identified in a number of ore samples from Bogosu and Prestea. Tetrahedrite occurs most frequently as inclusions within either pyrite or chalcopyrite and also in minor quantities as separate grains interspersed with other sulphides in the ores. Eighteen grains of tetrahedrite from Bogosu and Prestea were analysed by EMP (Table 5). There was no appreciable difference in composition between inclusions and separate grains. One tetrahedrite grain contained a microscopic inclusion of gold, and all grains contained minor "invisible" Au values ranging from 0.0 to 0.3 wt % Au at Bogosu, and from 0.1 to 0.5 wt % Au at Prestea.

The maximum recorded Ag content of Bogosu tetrahedrite was only 0.4 wt %, but, tetrahedrite from Bogosu has notably higher S, As and Cu values than tetrahedrite from Prestea. Grains from Prestea are considerably enriched in Ag (up to 17.4 wt % Ag), but also show higher Sb and Au values than tetrahedrite from Bogosu. Tetrahedrite compositions have a distinct bimodal distribution in an As/(As + Sb) vs Ag/(Ag + Cu) diagram (Fig. 8, Table 5). Grains from Bogosu ores plot within the normal tetrahedrite field, while those from Prestea ores plot along the Ag-rich Friebergite trend. All grains exhibit normal substitution patterns, with Ag exchanging for Cu, and As for Sb (Hackbarth and Petersen 1984; Ebel and Sack 1989).

The bimodal distribution in tetrahedrite mineral chemistry is similar to that reported by many investigators for both laboratory experiments and natural assemblages from polymetallic base-metal sulphide deposits and bonanza-type precious metal deposits (Wu and Petersen 1977; Hackbarth and Petersen 1984; Sack and Loucks 1985; Ebel and Sack 1989; Mishra and Mookherjee 1991). These studies demonstrate that tetrahedrite may be an excellent sliding-scale indicator for physico-chemical changes in the environment of ore deposition, particularly for variations in metal and semi-metal element concentrations in the ore fluid. The Ag content of tetrahedrite is apparently primarily a function of the aAg^+/aCu^+ in the ore fluid, and of the proportion of Sb to As. Both must be high for Ag-rich tetrahedrite. Based on tetrahedrite composition, the concentration of Ag, Sb, Au and possibly Zn in the ore fluid

Table 3. Summary of microscopic gold distribution in Bogosu and Prestea ores

Total gold distribution by quantity (%)

District	In sulphides	In gangue
Bogosu	90	10
Prestea	67	33

Total gold distribution by size (μm)

District	Size range	Average grain size
Bogosu	0.5–35	7
Prestea	0.5–92	8

Distribution of gold associated with sulphide/arsenide minerals (%)

District	In pyrite	In arsenopyrite	In cpy, sph etc.
Bogosu	89	11	0
Prestea	31	49	20

Distribution of gold associated with sulphide/arsenide minerals (%)

District	Within grain	At grain margins
Bogosu	95	5
Prestea	77.5	22.5

Polished thin sections analysed = 42
Polished thin sections with microscopic gold = 30
Total number of microscopic gold grains detected = 563

Table 4. Mineral chemistry of gold (EMP wt %)

District	Ore type	Sample	Au	Ag	Hg	Cu	Total
Bogosu	CDO	C-11-1	91.7	2.9	1.1	0.1	95.8
Bogosu	CDO	C-11-2	94.2	3.7	1.1	0.3	99.2
Bogosu	CDO	C-11-3	91.0	1.2	0.5	0.2	92.9
Bogosu	CDO	C-11-4	93.8	2.9	1.1	0.1	98.0
Bogosu	GCZ	DM-3-5	88.1	7.5	0.5	0.1	96.2
Bogosu	GCZ	DM-3-6	91.2	6.4	0.5	0.1	98.1
Bogosu	GCZ	DM-3-7	88.2	7.6	0.6	0.1	96.4
Bogosu	CDO	DM-11-8	95.4	3.7	0.1	0.0	99.2
Bogosu	CDO	DM-11-9	95.7	2.7	0.2	0.1	98.7
Bogosu	CDO	DM-11-10	89.4	2.6	0.1	0.1	92.2
Bogosu	CDO	DM-11-11	93.6	3.4	0.1	0.0	97.2
Bogosu	CDO	DM-11-12	94.8	3.2	0.1	0.0	98.1
Bogosu	CDO	DM-11-13	94.4	4.3	0.0	0.1	98.7
Bogosu	GCZ	D-10-14	93.4	4.8	0.8	0.3	99.3
Prestea	CDO	P-28-15	86.3	11.0	0.0	0.0	97.2
Prestea	CDO	P-28-16	87.2	11.8	0.1	0.0	99.1
Prestea	CDO	P-28-17	85.1	11.7	0.0	0.5	97.3
Prestea	QVO	P-2-18	69.9	20.6	0.4	0.1	91.0
Prestea	QVO	P-2-19	73.4	21.1	0.3	0.0	94.8
Prestea	QVO	P-2-20	74.4	19.8	0.5	0.3	95.1
Prestea	QVO	P-2-21	77.4	17.3	0.3	0.0	95.1
Prestea	QVO	P-2-22	77.0	21.3	0.5	0.1	98.8
Prestea	GFO	P-30-23	73.9	18.4	0.4	0.0	92.8
Prestea	GFO	P-30-24	73.8	20.5	0.4	0.0	94.7
Prestea	GFO	P-30-25	76.6	20.3	0.5	0.0	97.5
Prestea	GFO	P-19-26	90.0	7.6	0.5	0.1	98.2

C, Chujah deposit, Bogosu; D, DM, Dumassie deposit, Bogosu; P, Prestea mine
CDO, carbonated dike ore; GCZ, graphitic crush zone ore
GFO, graphitic fissure ore; QVO, quartz vein ore

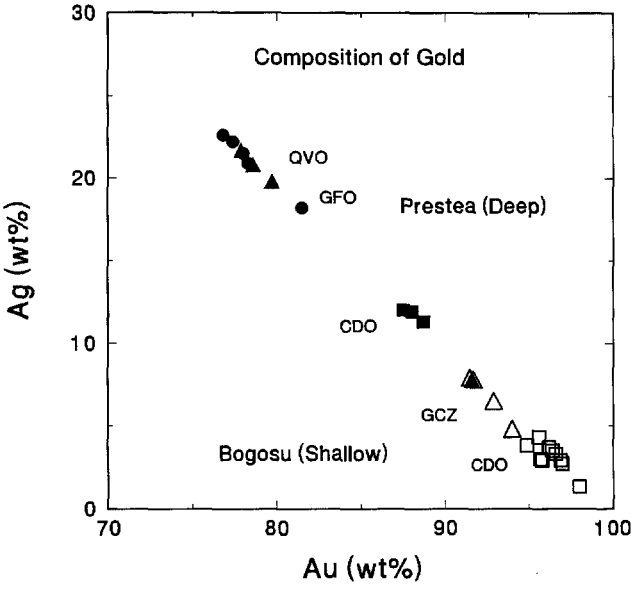

Fig. 7. Silver and Au contents of gold grains from Bogosu and Prestea ores. Both graphitic fissure ores (*GFO*) and crack-seal quartz vein ores (*QVO*) are associated with sedimentary rocks and have similar geochemical signatures. Note that both host-rock and depth of mineralization influence the Au to Ag ratios, with higher Ag contents in sedimentary rocks and in the structurally deeper ores of Prestea. The Au and Ag data of Table 4 are recalculated to 100% for this diagram: *CDO* is carbonated-dike ore; *GCZ* is graphitic "crush zone" ore; *QVO* is crack-seal quartz vein ore; *GFO* is graphitic fissure ore; Bogosu (*open symbols*); Prestea (*closed symbols*)

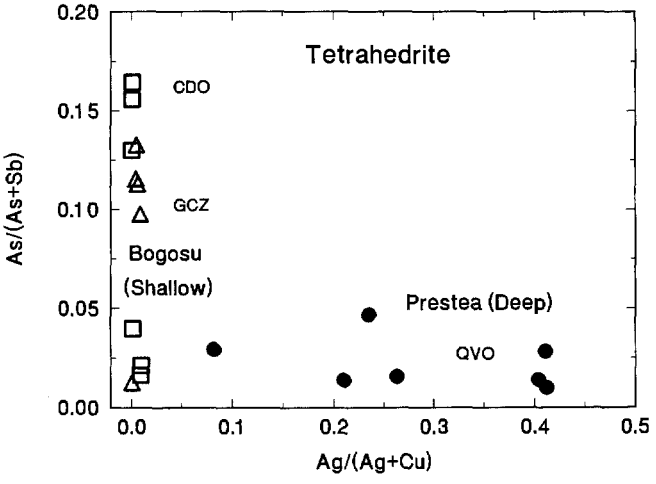

Fig. 8. Distinctive tetrahedrite mineral chemistries of Bogosu and Prestea ore. See Fig. 6 for legend

may have been decreasing during ascent through the zone of gold deposition in the Bogosu-Prestea gold system.

"Invisible" gold

"Invisible" gold was sporadically detected above background levels by EMP analysis of sulphide/arsenide minerals in Bogosu and Prestea ores. Individual spot analyses

Table 5. Mineral chemistry of tetrahedrite (EMP wt %)

District	Ore type	Sample	Au	Ag	S	As	Cu	Zn	Fe	Sb	Pb	Total
Bogosu	GCZ	DM-3-1	0.2	0.2	24.6	3.2	38.3	2.6	5.0	24.6	0.0	98.6
Bogosu	GCZ	DM-3-2	0.1	0.2	23.9	3.1	37.6	2.8	4.0	24.3	0.0	96.0
Bogosu	GCZ	DM-3-3	0.0	0.3	29.2	2.1	29.6	2.6	13.4	19.6	0.0	96.8
Bogosu	GCZ	DM-3-4	0.0	0.0	27.5	0.3	41.2	0.0	2.7	26.4	0.0	98.0
Bogosu	GCZ	DM-3-5	0.1	0.2	23.8	3.6	36.8	3.1	6.3	23.7	0.0	97.5
Bogosu	CDO	DM-11-6	0.1	0.0	29.1	3.2	41.1	0.1	3.1	21.6	0.1	98.3
Bogosu	CDO	DM-11-6	0.1	0.0	29.1	3.9	42.6	0.0	1.7	21.3	0.1	98.8
Bogosu	CDO	DM-11-7	0.2	0.0	25.0	4.5	38.5	3.8	4.1	22.7	0.0	98.9
Bogosu	CDO	DM-11-8	0.3	0.1	24.5	1.1	38.0	6.8	1.6	27.3	0.0	99.6
Bogosu	CDO	DM-11-9	0.3	0.4	24.0	0.5	36.7	3.1	5.7	27.9	0.0	98.4
Bogosu	CDO	DM-11-9	0.0	0.4	24.1	0.6	36.3	2.9	5.7	27.4	0.0	97.4
Prestea	QVO	P-2-10	0.3	17.4	21.9	0.3	24.9	4.0	3.2	27.0	0.0	99.0
Prestea	QVO	P-2-11	0.1	9.4	22.5	1.3	30.5	3.2	3.4	26.2	0.0	96.5
Prestea	QVO	P-2-12	0.3	10.5	22.3	0.4	29.3	3.5	4.1	27.5	0.0	97.9
Prestea	QVO	P-2-13	0.5	17.2	21.7	0.4	25.4	2.8	4.9	26.7	0.0	99.6
Prestea	QVO	P-2-14	0.2	8.2	23.2	0.4	30.9	3.0	6.5	25.3	0.0	97.6
Prestea	QVO	P-2-15	0.2	3.1	22.8	0.8	35.1	3.1	3.5	27.7	0.0	96.3
Prestea	QVO	P-2-16	0.3	17.1	21.8	0.8	24.6	2.5	3.9	26.1	0.0	97.1
Standard	NA	NA	0.0	0.1	25.1	0.1	42.5	0.0	3.3	29.3	0.0	100.4
Standard	NA	NA	0.1	0.1	24.5	0.1	42.5	0.0	3.4	29.2	0.0	99.7

CDO, Carbonated dike ore; GCZ, graphitic crush zone ore; QVO, quartz vein ore
DM, Dumassie deposit, Bogosu; P, Prestea mine

using a beam diameter of about 2.5 μm yielded values of up to 0.1 wt % "invisible" gold in both pyrite and arsenopyrite. Gold values ranged up to 0.5 wt % in tetrahedrite and above 1.0 wt % in boulangerite and stibnite.

Previous investigators (e.g., Cathelineau et al. 1989; Cabri et al. 1989; Bakken et al. 1989; Cook and Chryssoulis 1990; Chryssoulis and Cabri 1990; Fleet et al. 1993) demonstrated that sub-microscopic gold exists in arsenopyrite and arsenian pyrite both in solid solution in the crystal lattice and as discrete colloidal particles. Gold was preferentially concentrated within As-rich zones of arsenian pyrite (Fleet et al. 1993) and in As-rich and (Sb + Fe)-poor zones of arsenopyrite (Cathelineau et al. 1989). The concentration of "invisible" gold ranges up to 1,000 ppm in pyrite from the Fairview deposit, R. S. A. (Fleet et al. 1993) and 15,200 ppm in arsenopyrite from Chatelet and Villeranges, France (Marcoux et al. 1989). In the present study, sample DM-11 is a gold-rich sample of carbonated-dike ore from the Dumassie deposit in the Bogosu concession, and sample P-19 is representative of gold-rich fissure and quartz vein ores from Prestea (Table 6). In addition to "invisible" gold, polished thin sections of the same samples contained 99 (DM-11) and 69 (P-19) discrete grains of microscopic gold ranging in size from 0.5 to 32 μm and 0.5 to 48 μm, respectively. The concentration of "invisible" gold within arsenopyrite grains of the Bogosu sample was consistently high and ranged from 16 to 280 ppm Au. This contrasts with low values obtained from 3 arsenopyrite grains at Prestea that ranged from 0.56 to 1.0 ppm gold (Table 6). In spite of low gold values in the Prestea sulphides, discrete colloidal gold particles were detected in ion maps of these grains (e.g., Fig. 9).

A similar pattern of high "invisible" gold-contents (from 0.16 to 330 ppm Au) was detected in Bogosu pyrite, while 6 grains of pyrite from Prestea yielded consistently lower values of from 0.14 to 3.1 ppm Au (Table 6). At Bogosu, smaller grains had distinctly lower "invisible" gold contents with only 0.16 and 0.37 ppm in grains #6 and #7, respectively (Table 6), which were only about 0.1 mm in diameter. Also, the late outer growth zone of As-poor

Table 6. "Invisible" Au concentration in representative sulphide/arsenide minerals from Bogosu and Prestea ores (by SIMS)

District	Mineral	Analysis no.	Au (ppb)
Bogosu	Pyrite	DM-11-5	15000
Bogosu	Pyrite	DM-11-6	370
Bogosu	Pyrite	DM-11-7	160
Bogosu	Pyrite	DM-11-9	14000
Bogosu	Pyrite	DM-11-10	78000
Bogosu	Pyrite	DM-11-11	115000
Bogosu	Pyrite	DM-11-12	330000
Bogosu	Pyrite	DM-11-13	115000
Bogosu	Pyrite	DM-11-14	1500
Bogosu	Pyrite	DM-11-20	5900
Bogosu	Pyrite	DM-11-21	19000
Bogosu	Arsenopyrite	DM-11-1	280000
Bogosu	Arsenopyrite	DM-11-2	16000
Bogosu	Arsenopyrite	DM-11-3	93000
Bogosu	Arsenopyrite	DM-11-4	106000
Bogosu	Arsenopyrite	DM-11-8	29000
Bogosu	Arsenopyrite	DM-11-15	80000
Bogosu	Arsenopyrite	DM-11-16	21000
Bogosu	Arsenopyrite	DM-11-17	67000
Bogosu	Arsenopyrite	DM-11-18	144000
Bogosu	Arsenopyrite	DM-11-19	83000
Prestea	Pyrite	P-19-1	3100
Prestea	Pyrite	P-19-2	1000
Prestea	Pyrite	P-19-3	1800
Prestea	Pyrite	P-19-6	160
Prestea	Pyrite	P-19-8	140
Prestea	Pyrite	P-19-9	740
Prestea	Arsenopyrite	P-19-4	1000
Prestea	Arsenopyrite	P-19-5	600
Prestea	Arsenopyrite	P-19-7	560

DM-11, Dumassie deposit, Bogosu; carbonated-dike ore
P-19, Prestea mine; graphitic fissure ore

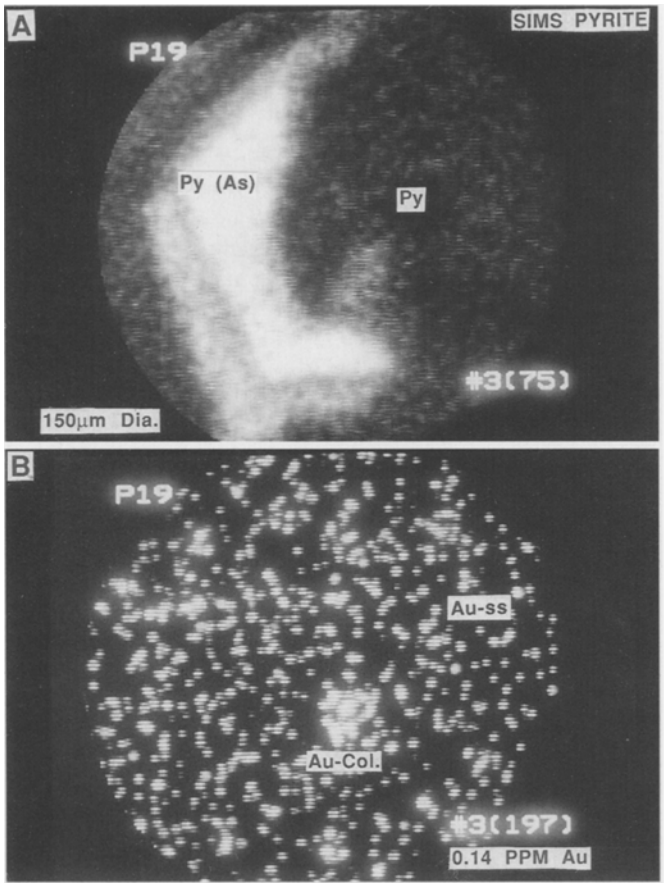

Fig. 9A, B. SIMS ion maps of distribution of ^{75}As and ^{197}Au in an arsenian pyrite grain from graphitic fissure ore in the Prestea mine (sample P-19). **A** ^{75}As ion map showing strong zoning in As content along pyrite growth bands. **B** Corresponding ^{197}Au ion map showing an evenly distributed low concentration (0.14 ppm) of gold. There is no apparent correlation between the content of gold in solid solution and the strong As zoning. Note the single colloidal particle of gold

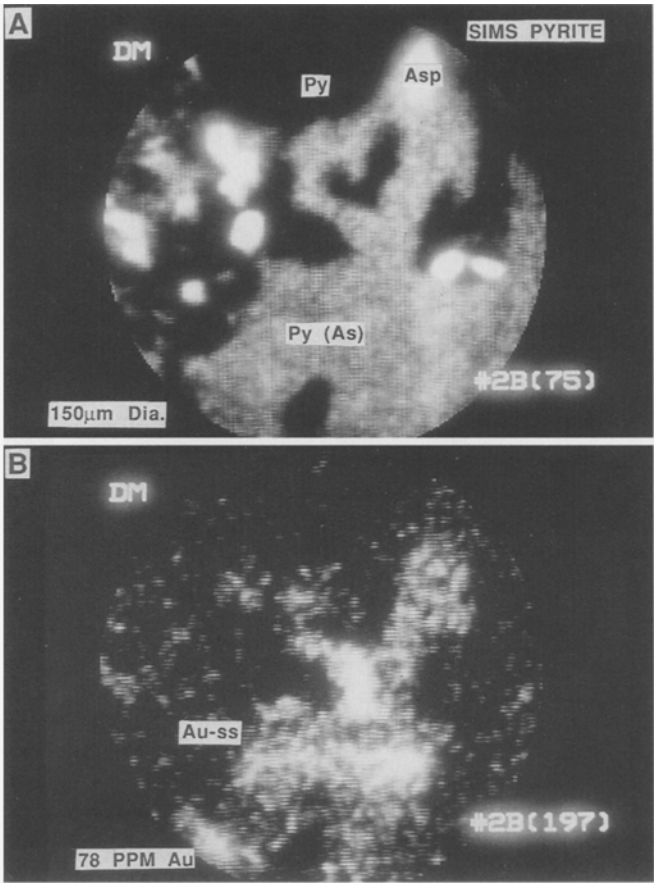

Fig. 10A, B. SIMS ion maps of distribution of ^{75}As and ^{197}Au in an arsenian pyrite grain from a sample of carbonated-dike ore from the Dumassie deposit, Bogosu concession (*sample DM-11*, #2B). The ions maps are from the As-rich band of the arsenian pyrite grain illustrated in Fig. 4C and 4D. **A** ^{75}As ion map showing a mosaic pattern of recrystallization of arsenian pyrite [Py (As)] to As-poor pyrite, pyrrhotite and arsenopyrite (*Asp*) microcrystals. **B** Corresponding ^{197}Au ion map showing that Au is concentrated (*78 ppm*) in solid solution (*Au-ss*) in the non-recrystallized, As-rich portions of the pyrite crystal. Recrystallized portions of the pyrite grain are As-poor and noticeably depleted in Au

pyrite of the grain shown in Figure 5C had only 1.5 ppm gold (analysis #14, Table 6). The highest gold values in pyrite at Bogosu and Prestea were in the larger, As-rich porphyroblastic grains that often exceed 1.0 mm in diameter. Examples include the pyrite grain shown in Figures 5C and 10, and analyses #5, #9, #14, #20 and #21 for Bogosu and grain #1 for Prestea (Table 6).

From the SIMS ion mapping in the Bogosu ores, Au in solid solution within the pyrite lattice is clearly associated with As-rich zones (Fig. 10). However, gold occurs also as discrete colloidal size (≈ 0.001 to 0.1 μm) particles that may be in either As-rich zones (Fig. 10) or As-poor zones (Fig. 11). The core of the pyrite porphyroblast shown in Figures 5C and 5E is composed of early, As-poor pyrite that altered from pre-existing pyrrhotite and marcasite. This core region does not contain Au, with the exception of minor colloidal-size microinclusions that formed along grain boundaries or micro-fractures. These early grains are cemented together by arsenian pyrite which does contain Au in solid solution. In the Prestea sample, pyrite grains have As-rich zones that are at least as prominent as those in pyrite from Bogosu. However, in the Prestea grains the distribution of "invisible" gold clearly does not correlate with As-rich bands in some grains (e.g., Fig. 9), and in others the correlation is barely discernible. This feeble correlation of Au with As in Prestea pyrite may be attributable to their low Au content.

Two generations of arsenopyrite occur as inclusions in pyrite. Subhedral arsenopyrite microcrystals associated with recrystallized As-depleted mosaics of iron sulphides in As-rich zones of arsenian pyrite are distinctly Au-poor (e.g., Fig. 10). An earlier generation of independently-nucleated arsenopyrite grains in pyrite porphyroblasts tend to be Au-rich (e.g., 144 ppm Au from analysis #15, Table 6).

The larger arsenopyrite crystals at Bogosu have high invisible Au content (up to 280 ppm) and the distribution of Au is strongly zoned in growth bands. In some grains a direct relationship of Au to distribution of As and S is not established since subtle compositional variations in S and As are not well resolved in the SIMS images.

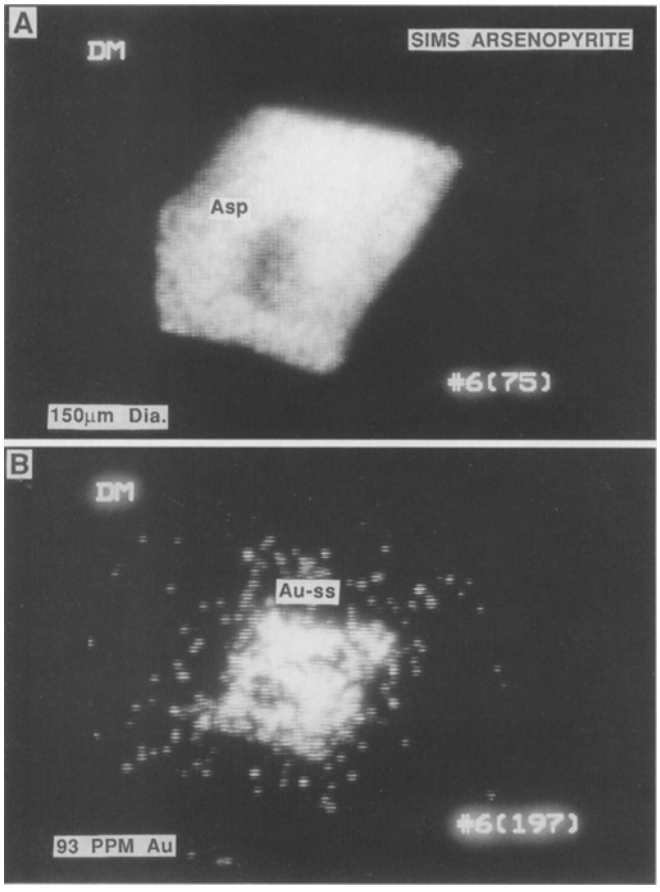

Fig. 11A, B. SIMS ion maps of distribution of ^{75}As and ^{197}Au in an arsenopyrite grain from a sample of carbonated-dike ore from the Dumassie deposit, Bogosu concession (*sample DM-11, #6*). **A** ^{75}As ion map showing the distribution of As. EMP BSE images of the same grain demonstrate that the outer growth band of this arsenopyrite crystal is As-rich with-respect-to the core region. **B** Corresponding ^{197}Au ion map showing Au in solid solution concentrated in the As-poor core of the euhedral arsenopyrite crystal

However, in others, such as that illustrated in Fig. 11, Au is clearly concentrated in the core region (93 ppm Au), which is surrounded by an Au-poor rim. From back-scattered electron images, the core of this grain is As-poor, and the margin As-rich. This clearly demonstrates that higher Au values in arsenopyrite are not, in all cases, associated with zones of higher As content. According to the arsenopyrite and carbonate mineral geothermometry (Mumin 1994; Mumin and Fleet 1994), formation temperatures indicated by As concentrations in the outer margin of this grain (Fig. 11) were too high ($\approx$ 450°C) for gold deposition in the Bogosu-Prestea system, whereas, temperatures indicated by the core region ($\approx$ 340°C) do fall within the expected temperature range for gold precipitation.

Precipitation and evolution of gold in the Bogosu-Prestea system

The occurrence of gold in a variety of modes within a single gold system leads to some interesting conclusions regarding gold precipitation, distribution and evolution. The evidence from Bogosu and Prestea suggests that virtually all gold initially precipitated as a solid solution with arsenian pyrite and arsenopyrite, and to a much lesser extent with tetrahedrite, and possibly some of the other sulphides in the system. The paragenetic sequence (Fig. 4) indicates that gold in solid solution precipitated almost entirely during the arsenian event of the Stage 3 hydrothermal alteration, the same event that produced the compositional zoning of arsenian pyrite and arsenopyrite. This reconstruction appears different to Bonnemaison and Marcoux (1990) who suggested that in gold systems including vein types (e.g., Poura, Burkina Faso), "porphyries" (e.g., Loulouie, Guyana) and stockwork deposits (e.g., Le Chatelet, France) gold originally precipitated in solid-solution with early-formed pyrrhotite, and subsequently altered and recrystallized as Au-bearing pyrite and arsenopyrite.

At Bogosu and Prestea, there does not appear to be any evidence to associate gold with pyrrhotite crystallization. Apparently, the conversion of pyrrhotite to pyrite and marcasite was by a solution-precipitation mechanism rather than from sulphidation in the solid state, as is evident from the random product crystal orientations (Murowchick 1990; Schoonen and Barnes 1991a, 1991b). The former process will proceed very efficiently at temperatures below 200 to 250°C, where the solubility product of pyrite is six to ten orders of magnitude less than that of pyrrhotite (Naumov et al. 1974). Hence, re-precipitation of pyrite will occur almost immediately upon dissolution of pyrrhotite when accompanied by a slight oxidation of the sulphide to polysulphide. If the pH is below 5, marcasite will form rather than pyrite (Murowchick and Barnes 1986; Murowchick 1992). Under these conditions of: 1) increasing oxidation state from pyrrhotite stability to pyrite stability, 2) increasing pH from below to above 5, and 3) temperatures of about 250 °C, Romberger (1989) demonstrated that the solubility of Au will increase by up to several orders of magnitude. This is consistent with the findings of this study and further indicates that it is very unlikely that gold could have originally precipitated during the early formation of pyrrhotite, marcasite and pyrite.

After precipitation of gold as a trace and minor constituent in arsenian pyrite and arsenopyrite, its redistribution and crystallization commenced almost immediately and proceeded with more or less efficiency, depending upon the post-precipitation metamorphic and hydrothermal conditions, deformation, and refractory properties of the host minerals. Consequently, in a large system such as the Bogosu-Prestea gold system, various stages of gold redistribution and concentration are preserved.

At Bogosu, local diffusion of major components and recrystallization of arsenian pyrite are clearly documented by the formation of arsenopyrite and pyrrhotite microcrystals from As-rich zones (Figs. 5C, 5D and 10), and the growth of As-depleted areas within pyrite. The recrystallized, As-poor areas in pyrite are also depleted in gold, as are the newly-formed arsenopyrite and pyrrhotite microcrystals. Gold in solid-solution is found in quantity only in relict arsenian portions of the pyrite, as is illustrated in Figure 10. Most importantly, local concentration of gold now occurs, and invisible but discrete colloidal gold

particles form in relative abundance along the grain contacts of As-poor pyrite with or without relict arsenian pyrite. With further evolution of the deposit, remobilization of gold in solid-solution becomes much more extensive and some colloidal inclusions grow to microscopic sizes.

However, at Prestea, the redistribution and concentration of gold is not restricted to areas of recrystallization of arsenian pyrite, arsenopyrite and pyrrhotite, but appears to be ubiquitous in all pyrite and arsenopyrite grains examined. For example, prominent compositional zoning is preserved in Prestea grains as in most of the Bogosu sulphides, yet the SIMS ion maps indicate that gold has effectively redistributed and concentrated into discrete colloidal, microscopic and visible particles. This evidence suggests that at least some of the gold may have redistributed without recrystallization of arsenian pyrite or arsenopyrite, perhaps through some form of diffusion (infiltration) mechanism.

The observed remobilization of gold in the Bogosu-Prestea gold system follows a distinctive pattern (Fig. 12). Initially, gold in solid solution migrated towards fractures and voids within the sulphides, then to grain margins, and ultimately out of the host sulphide crystals, to be reprecipitated interstitial to gangue minerals where it appears to have a long residence time. In the more extreme cases illustrated by the Prestea sulphides, most of the gold appears to have migrated out of solid solution with sulphides, leaving behind minor values and only weak remnant correlations to strong compositional zoning in As content. At Bogosu, the minimal "invisible" gold contents of small arsenian pyrite grains indicate that gold will migrate more readily out of small grains, while being trapped as colloidal and microscopic particles in larger grains. However, in some arsenopyrite and arsenian pyrite grains gold seems to have preferentially migrated to the grain core, particularly to sieve-textured cores (e.g. Fig. 5A). This pattern of gold redistribution may have been influenced by permeability created by microfractures, as expected for infiltration-dominated diffusion.

As demonstrated elsewhere (Mumin 1994; Mumin and Fleet 1994), ambient country-rock metamorphic conditions as well as temperatures of mineralization were moderately higher at Prestea than Bogosu during and subsequent to mineralization. This is believed to be a major factor promoting the more extensive recrystallization and redistribution of gold at Prestea after the initial precipitation in sulphide minerals. It is apparent that higher-grade metamorphic/hydrothermal conditions during and/or after precipitation led to more efficient recrystallization and redistribution of gold, and to its eventual migration into the gangue assemblages. The better preservation of primary gold distribution at Bogosu must be attributable to the higher level of Bogosu ores in the gold system and the slightly-lower grade of metamorphism that affected this district during and after mineralization.

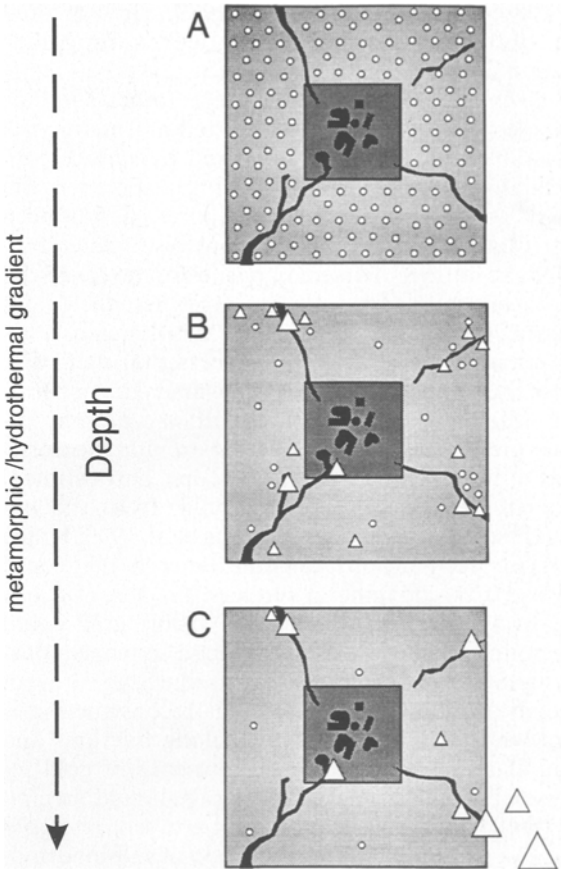

Fig. 12A–C. Schematic diagram illustrating the redistribution and concentration of invisible Au in sulphide/arsenide minerals in the Bogosu-Prestea gold system. **A** Primary deposition of invisible Au in solid-solution with sulphide/arsenide minerals. **B** Redistribution and concentration of solid-solution Au to form colloidal and microscopic particles in fractures and voids within the host minerals. **C** Further concentration and migration of solid-solution, colloidal and microscopic Au to form larger particles in voids and fractures, and eventually migrate out of the host mineral and interstitial to gangue minerals where the gold appears to have a long residence time

Concentration and precipitation of gold

The precipitation of gold from the ore fluids into structurally bound solid-solution with sulphide/arsenide minerals could account quantitatively for the observed distribution patterns and modes of occurrence of gold documented at Bogosu and Prestea. On mass balance grounds, for example, a 1 mm cube of arsenian pyrite or arsenopyrite averaging 100 ppm "invisible" gold would yield a single particle of gold about 30 μm in diameter. In other deposits, the averaged "invisible" gold contents of some arsenian pyrite and arsenopyrite grains locally range as high as 1000 ppm and 4,900 ppm, respectively, (Fleet et al. 1993; Marcoux et al. 1989). Contents as high as these would increase the potential volume of gold metal by at least another order of magnitude over the above calculation.

The precise mechanism by which gold is precipitated along with sulphides has not been addressed in this study. However, many investigators have shown that Au, Ag, As, Sb, Hg and possibly other metals are readily and abundantly carried as bisulphide complexes (e.g., $Au(HS)_2^-$) in hydrothermal solutions (Barnes 1979;

Seward 1989; Seward and Barnes 1989; Hayashi and Ohmoto 1991). Precious metals carried as bisulphide complexes may be incorporated into the crystal lattice of growing arsenian pyrite, arsenopyrite or other sulphide minerals. Fleet et al. (1989) suggested that arsenian pyrite was metastable and that gold was fixed by surface-controlled reactions onto faces of growing arsenian pyrite crystals. In sedimentary-rock hosted ores, it has been suggested that deposition of gold from bisulphide complexes into the lattices of arsenian pyrite and arsenopyrite may result from coupled redox reactions, where the gold is oxidized and thioarsenide species are simultaneously reduced (Arehart et al. 1993). Any process that would fix gold onto the surface of sulphide or arsenide minerals during crystal growth is consistent with the present findings. The present discussion does not exclude the possibility that at least some of the microscopic and colloidal gold accumulated directly, as free gold, from the hydrothermal fluid by adsorption (Starling et al. 1989; Knipe et al. 1991) or precipitation (Jean and Bancroft 1985) onto sulphide and arsenide mineral surfaces.

Alternatively, the microscopic and visible gold could have precipitated late in the paragenetic sequence, possibly during Stage 4, and separate from the Stage 3 event that precipitated "invisible" gold. This reconstruction is consistent with the presence of gold along fractures and grain boundaries, but not with the presence of gold inclusions isolated within sulphide minerals. If gold precipitated at this late stage it would require a separate gold event without simultaneous precipitation of sulphide minerals. It would also be necessary to explain why this late-stage gold only precipitated on arsenian pyrite, and not on As-poor pyrite, marcasite and pyrrhotite. The direct accumulation of larger gold particles does not appear to be consistent with observations at Bogosu and Prestea, where sulphide mineral growth occurred before, during and after gold precipitation (Fig. 4.). Also, the weight of evidence from experimental and theoretical calculations shows that gold solubilities in mesothermal hydrothermal systems fall within the stability range of common sulphide minerals such as pyrrhotite, pyrite and arsenopyrite (e.g., Drummond and Ohmoto 1985; Romberger 1989; Shenberger and Barnes 1989). Hence, major episodes of gold precipitation without simultaneous sulphide mineral growth may be rare in natural systems.

We recognize that the low "invisible" gold content of arsenian pyrite at Prestea could be a primary feature. At this depth in the gold system during stage 3 alteration and mineralization, proportionally more gold could have been precipitated as microscopic and visible Au and less as lattic-bound solid solution in the sulphide/arsenide minerals.

Conclusions for ore genesis

The results of this investigation present compelling evidence that primary gold deposition in the Bogosu-Prestea gold system was mostly in the form of solid-solution with arsenian pyrite, arsenopyrite and other sulphide/arsenide minerals. Gold particles in late fractures and voids in sulphide and arsenide minerals resulted from post-depositional redistribution of gold formerly held in solid-solution. The common presence of gold in late fractures is clearly insufficient evidence to suggest that gold was introduced at a late stage in the evolution of mesothermal gold systems.

The difference in erosional level between Bogosu and Prestea ores has exposed both structurally higher and structurally deeper portions of a giant gold system, allowing documentation of gold distribution in relationship to several physical and chemical parameters. The distribution and morphology of gold in solid-solution and as colloidal, microscopic and large particles resulted from post-depositional, almost *in-situ*, redistribution and concentration. Redistribution of gold is believed to have commenced immediately after deposition; however, we believe redistribution continued throughout the post-depositional history of these deposits. Gold redistribution and concentration progressed from solid-solution gold to colloidal and microscopic particles within host minerals, and eventually to larger particles at grain margins and in gangue. Current evidence suggests that the amount of post-depositional redistribution increased with: 1) increasing hydrothermal and metamorphic grade, 2) decreasing refractory properties of host minerals, 3) increasing deformation, 4) increasing recrystallization of host minerals, 5) decrease in grain size, and 6) the degree to which host minerals communicated with hydrothermal solutions. We note that there is an increase in the redistribution of gold with depth, but recognize that exceptions to this correlation might occur in dynamic giant gold systems depending on permeability, deformation and mineralogy of different lodes.

We suggest that the general conclusions presented here from investigations of a giant gold system in the Early Proterozoic Birimian of West Africa are applicable to As-rich gold deposits of all ages, worldwide, and all such deposits should be re-evaluated in the light of these new findings. Our results may not be applicable to As-poor mesothermal gold deposits, which apparently have little primary gold in solid solution in pyrite. However, redistribution of particulate gold must be a continuing phenomenon in these deposits also.

Implications for metallurgy and exploration

The metallurgical implications for the presence of "invisible" gold in sulphide and arsenide minerals are potentially very significant. Ten weight percent of sulphide in a gold ore averaging 100 ppm of "invisible" gold will contribute 10 g/t to the overall grade of a gold deposit. Also, it is unclear how much of the "invisible" gold content of gold deposits is routinely and accurately detected by the assay techniques currently in use. "Invisible" gold is refractory to conventional extraction methods, and to our knowledge has not been metallurgically tested for recovery at Bogosu and Prestea. This gold fraction will not be recovered by direct cyanidation. Alternatively, mill recoveries may fluctuate unexpectedly and without apparent reason due to changing proportions of microscopic and visible gold to "invisible" gold. Based on analyses

presented in this and other studies, it is clear that a potential resource is being lost in some mines, since the "invisible" gold fraction may be partially non-detectable, and largely non-recoverable by the quantification and extraction techniques used by many mines.

The potential resource of "invisible" gold in a number of existing gold mining districts cannot be overstated, particularly where metamorphic, depth and/or hydrothermal gradients can be determined by other geological means. In this way, geologists can document where free-milling gold grades into refractory microscopic gold, and then extrapolate to and predict areas where concentrations of undetected solid-solution gold might exist.

Acknowledgements. We thank the two journal referees for helpful comments, and Sikaman Gold Resources, Billiton Bogosu Gold and Prestea Goldfields Limited for permission to conduct this research and providing logistical support. R.L. Barnett and D.M. Kingston assisted with the EMP analyses and C.G. Weisener performed the SIMS analyses. This research was supported by a Natural Sciences and Engineering Council of Canada research grant to M.E. Fleet.

References

Abouchami, W., Boher, M., Michard, A., Albarede, F. (1990) A major 2.1 Ga event of mafic magmatism in West Africa: An early stage of crustal accretion. J. Geophysical Res. 95:17,605–17,629

Adjimah, C.L. (1988) Petrological studies on the genesis of the gold deposits of Prestea, Ghana.Unpublished Thesis, Bundesanstalt fur Geowissenschaften und Rohstoffe, Hannover, 274 pp

Appiah, H., Norman, D.I. Boadi, I. (1991) The geology of the Prestea and Ashanti goldfields: a comparative study. In: Ladeira, E.A. (ed.) Brazil Gold 91. The economics, geology, geochemistry and genesis of gold deposits. pp. 247–255

Arehart, G.B., Chryssoulis, S.L., Kesler, S.E. (1993) Gold and arsenic in iron sulfides from sediment-hosted disseminated gold deposits: implications for depositional processes. Econ. Geol. 88:171–185

Bakken, B.M., Hochella, M.F., Jr., Marshall, A.F., Turner, A.M. (1989) High Resolution microscopy of gold in unoxidized ore from the Carlin mine, Nevada, Econ. Geol. 84:171–179

Barnes, H.L. (1979) Solubilities of ore minerals. In: Barnes, H.L. (ed.) Geochemistry of hydrothermal ore deposits 2nd edn. Wiley, New York, pp. 404–508

Bonnemaison, M. Marcoux, E. (1990) Auriferous mineralization in some shear-zones: a three-stage model of metallogenesis. Mineral Deposita 25:96–104

Cabri, L.J., Chryssoulis, S.L., De Villiers, J.P.R., Laflamme, J.H.G. Buseck, P.R. (1989) The nature of "invisible" gold in arsenopyrite. Can. Mineralogist 27:353–362

Cathelineau, M., Boiron, M.C., Hollinger, P. Marion, P. Denis, M. (1989) Gold in arsenopyrites: crystal chemistry, location and state, physical and chemical conditions of deposition. Econ. Geol. Monogr. 6:328–341

Chryssoulis, S.L., Cabri, L.J. (1990) Significance of gold mineralogical balances in mineral processing. Trans. Inst. Min. Metall. 99:C1–C10

Cook, N.J., Chryssoulis, L. (1990) Concentrations of ""invisible" gold" in the common sulfides. Can. Mineralogist 28:1–16

Drummond, S.E., Ohmoto, H. (1985) Chemical evolution and mineral deposition in boiling hydrothermal systems. Econ. Geol. 80:126–147

Ebel, D.S., Sack, R.O. (1989) Ag–Cu and As–Sb exchange energies in tetrahedrite-tennantite fahlores. Geochim. Cosmochim. Acta 53:2301–2309

Fleet, M.E., MacLean. P.J., Barbier, J. (1989) Oscillatory-zoned As bearing pyrite from strata-bound and stratiform gold deposits: An indicator of ore fluid evolution. Econ. Geol. Monogr. 6:356–362

Fleet, M.E., Chryssoulis, S.L., MacLean, P.J., Davidson, R., Weisener, C.G. (1993) Arsenian pyrite from gold deposits: Au and As distribution investigated by SIMS and EMP, and color staining surface oxidation by XPS and LIMS. Can. Mineralogist 31:1–17

Garard, T.F. (1989) Gold in Africa: jewellery and ornaments from Ghana, cote d'Ivoire, Mali and Senegal in the collection of the Barbier-Mueller Museum, Munich. Prestel, Munich New York, 247 pp

Goldfarb, R.J., Leach, D.L., Rose, S.C., Landis, G.P. (1989) Fluid inclusion geochemistry of gold-bearing quartz veins of the Juneau gold belt, southwestern Alaska. Econ. Geol. Monogr. 6:363–375

Goldfarb, R.J., Newberry, R.J., Pickthorn, W.J., Gent, C.A. (1991) Oxygen, hydrogen, and sulfur isotope studies in the Juneau Gold Belt, south-eastern Alaska: constraints on the origin of hydrothermal fluids. Econ. Geol. 86:66–80

Hackbarth, C.J., Petersen, U. (1984) Systematic compositional variations in argentian tetrahedrite. Econ. Geol. 79:448–460

Hastings, D.A. (1982) On the tectonics and metallogenesis of West Africa: a model incorporating new geophysical data. Geoexploration 20:295–327

Hayashi, K.-I., Ohmoto, H. (1991) Solubility of gold in NaCl and H_2S-bearing aqueous solutions at 250–350 °C. Geochim. Cosmochim. Acta 55:2111–2126

Haynes, S.J. (1986) Geology and chemistry of turbidite-hosted gold deposits, greenschist facies, eastern Nova Scotia. In: Keppie, J.D., Boyle, R.W., Haynes, S.J. (eds.) Turbidite-hosted gold deposits. GAC Special Paper 32: 161–178

Jean, G.E., Bancroft, G.M. (1985) An XPS and SEM study of gold deposition at low temperatures on sulphide mineral surfaces: concentration of gold by adsorption/reduction. Geochim. Cosmochim. Acta 49:979–987

Junner, N.R. (1940) Geology of the Gold Coast and Western Togoland. Ghana Geol. Survey Bull. 11:40 pp

Kerrich, R., Wyman, D. (1990) Geodynamic setting of mesothermal gold deposits: an association with accretionary tectonic regimes. Geology 18:882–885

Kesse, G.O. (1985) The mineral and rock resources of Ghana. Balkema, Rotterdam, 610 pp

Klemd, R., Hirdes, W., Olesch, M., Oberthur, T. (1993) Fluid inclusions in quartz-pebbles of the gold-bearing Tarkwaian conglomerates of Ghana as guides to their provenance area. Mineral. Deposita 28:334–343

Knipe, S.W., Foster, R.P. (1991) Hydrothermal precipitation of precious metals on sulfide substrates. In: Ladeira, E.A. (ed.) Brazil Gold 91. The economics, geology, geochemistry and genesis of gold deposits. pp 431–435

Knopf, D.J. (1988) Gold in West Africa and the Ivory Coast. Mining Magazine 158:392–396

Kontak, D.J., Smith, P.K. (1993) A metaturbidite-hosted lode gold deposit: the Beaver Dam deposit, Nova Scotia. 1. Vein paragenesis and mineral chemistry. Can. Mineralogist 31:471–522

Kretschmar, U., Scott, S.D. (1976) Phase relations involving arsenopyrite in the system Fe–As–S and their application. Can. Mineralogist 14:364–386

Leube, A., Hirdes, W., Mauer, R., Kesse, G.O. (1990) The early Proterozoic Birimian supergroup of Ghana and some aspects of its associated gold mineralization. Precambrian Res. 46:139–165

Marcoux, E., Bonnemaison, M., Braux, C., Johan, Z. (1989) Distribution de Au, Sb, As, et Fe dans l'arsenopyrite aurifere du Chatelet et de Villeranges (Creuse, Massif Central Francais). C. R. Acad. Sci. 308 II:293–300

Milesi, J.P., Ledru, P., Feybesse, J.L., Dommanget, A., Marcoux, E. (1992) Early Proterozoic ore deposits and tectonics of the Birimian orogenic belt, West Africa. Precambrian Res. 58:305–344

Mishra, B., Mookherjee, A. (1991) Tetrahedrite mineral chemistry and metal zoning: a thermodynamic assessment from the Rajpura-Dariba polymetallic deposit, India. Econ. Geol. 86:1529–1538

Mumin, A.H. (1994) Early Proterozoic Birimian gold mineralization of the Bogosu and Prestea districts of the Ashanti Gold Belt, Ghana, West Africa. Unpublished Ph.D. thesis, University of Western Ontario, London, Canada, 312 pp

Mumin, A.H., Fleet, M.E. (1994) Evolution of gold mineralization in the Ashanti Gold Belt, Ghana: evidence from carbonate compositions and paragenesis. Mineralogy Petrology (in press)

Mumin, A.H., Fleet, M.E., Longstaffe, F.J. (1994) Evolution of hydrothermal fluids in the Ashanti Gold Belt, Ghana: stable isotope geochemistry of carbonates, graphitic material and quartz. Econ. Geol. (submitted for publication)

Murowchick, J.B. (1990) Iron monosulfide precursors in low-temperature pyrite and marcasite formation (abstract). Geol. Soc. America 22: PA207

Murowchick, J.B. (1992) Marcasite inversion and the petrographic determination of pyrite ancestry. Econ. Geol. 87: 1141–1152

Murowchick, J.B., Barnes, H.L. (1986) Marcasite precipitation from hydrothermal solutions. Geochim. Cosmochim. Acta 50: 2615–2629

Naumov, G.B., Ryzhenko, B.N., Khodakovsky, I.L. (1974) Handbook of thermodynamic data. US Geol. Survey Report USGS-WRD-74-001, 328 pp

Romberger, S.B. (1989) Transport and deposition of precious metals in epithermal deposits. In: Romberger, S (ed.) Mechanisms of Gold transport and deposition in low temperature hydrothermal systems. National Centre for Management Research, University of Western Ontario, London, Ontario

Sack, R.O., Loucks, R.R. (1985) Thermodynamic properties of tetrahedrite-tennantites: constraints on the interdependence of the Ag–Cu, Fe–Zn, Cu–Fe, and As–Sb exchange reactions. Am. Mineralogisst 70: 1270–1289

Sandiford, M., Keays, R.R. (1986) Structural and tectonic constraints on the origin of gold deposits in the Ballarat Slate Belt, Victoria. In: Keppie, J.D., Boyle, R.W. Haynes, S.J. (eds.) Turbidite-hosted Gold deposits. GAC Special Paper 32: 15–24

Schoonen, M.A.A. Barnes, H.L. (1991a) Reactions forming pyrite and marcasite from solution. I. Nucleation of FeS_2 below 100°C. Geochim. Cosmochim. Acta 55: 1495–1504

Schoonen, M.A.A. Barnes, H.L. (1991b) Reactions forming pyrite and marcasite from solution. II. Via FeS precursors below 100°C. Geochim. Cosmochim. Acta 55: 1505–1514

Sestini, G. (1973) Sedimentology of a paleoplacer: the gold-bearing Tarkwaian of Ghana. In: Amstutz, G.C. Bernard, A.J. (eds.) Sedimentary ores. Springer, Berlin Heidelberg New York, pp. 275–305

Seward, T.M. (1989) The hydrothermal chemistry of gold and its implications for ore formation: boiling and conductive cooling as examples. Econ. Geol. Monogr. 6: 398–404

Seward, T.M. Barnes, H.L. (1989) Metal transport and deposition by hydrothermal ore fluids: an introduction. In: Barnes, H.L. Ohmoto, H. (eds.) Hydrothermal processes-application to ore genesis. Reidel Dordrecht

Sharp, Z.D., Essene, E.J. Kelly, W.C. (1985) A re-examination of the aresenopyrite geothermometer: pressure considerations and applications to natural assemblages. Can. Mineralogist 23: 517–534

Shenberger, D.M. Barnes, H.L. (1989) Solubility of gold in aqueous sulfide solutions from 150 to 350°C. Geochim. Cosmochim. Acta 53: 269–278

Starling, A., Gilligan, J.M., Carter, A.H.C., Foster, R.P. Saunders, R.A. (1989) High temperature hydrothermal precipitation of precious metals on the surface of pyrite. Nature 340: 298–300

Taylor, P.N., Moorbath, S., Leube, A. Hirdes, W. (1992) Early Proterozoic crustal evolution in the Birimian of Ghana: constraints from geochronology and isotope geochemistry. Precambrain Res. 56: 97–111

Wu, I. Petersen, U. (1977) Geochemistry of tetrahedrite and mineral zoning at casapalca, Peru. Econ. Geology 72: 993–1016

Editorial handling: R. Kerrich